Electronic supplementary information (ESI)

Interface Modification of Sputtered NiO_x as the Hole Transport Layer for Efficient Inverted Planar Perovskite Solar Cells

Xiaolu Zheng,†, [a], [b], [d] Zhaoning Song,†,*, [b] Zhiliang Chen,†, [a] Sandip Singh Bista,[b] Pengbin Gui, [a] Niraj Shrestha, [b] Cong Chen, [a], [b] Chongwen Li,[b] Xinxing Yin,[b] Rasha A. Awni,[b] Hongwei Lei,[c] Chen Tao,[a] Randy J. Ellingson,[b] Yanfa Yan,[b] Guojia Fang*, [a],[d]

[a] Key Lab of Artificial Micro- and Nano-Structures of Ministry of Education of China, School of Physics and Technology, Wuhan University, Wuhan 430072, P. R. China
Email: gjfang@whu.edu.cn

[b] Department of Physics and Astronomy and Wright Center for Photovoltaics Innovation and Commercialization, The University of Toledo, Toledo, OH, 43606, United States
Email: zhaoning.song@utoledo.edu

[c] College of Science, Huazhong Agricultural University, Wuhan 430070, P. R. China

[d] Shenzhen Institute, Wuhan University, Shenzhen 518055, P. R. China.

† These authors contributed equally.

Experimental section

Materials

Lead thiocyanate ($Pb(SCN)_2$), potassium chloride (KCl) and bathocuproine (BCP) were purchased from Sigma-Aldrich. [6,6]-phenyl-C61-butyric acid methyl ester (PCBM) was purchased from Nano-C. All organic solvents including *N*,*N*-dimethylformamide (DMF), dimethyl sulfoxide (DMSO), diethyl ether (DE), ethanol and chlorobenzene (CB) were also purchased from Sigma-Aldrich. Lead iodide (PbI_2) was purchased from TCI. Methylammonium iodide (MAI) and formamidinium iodide (FAI) were purchased from GreatCell Solar. All chemicals were used as received without further purification.

Deposition of NiO_x hole transport layer

NiO_x films were deposited by radio frequency magnetron sputtering of a 3″ NiO stoichiometric target (Lesker) in a Kurt J. Lesker Company ® PRO Line PVD system integrated in a glovebox. The target was pre-sputtered for 15 min before each deposition. To find the optimized deposition parameters we referred to the works reported by Aydin et al.[1], and the final parameters adopted in our case are listed as follow:

Parameter	Value
Base pressure	$<3\times10^{-7}$ Torr
Deposition pressure	3 mTorr
Sputtering power	90 W
Argon gas flow rate	15 sccm
Substrate temperature	Room temperature
Substrate rotation	10 rpm
Deposition rate	0.055 Å/s

Post-treatment of NiO_x films

Annealing. The NiO_x films were annealed on a hotplate at different temperatures in ambient air. The heating time was fixed at 30 min. After annealing, the samples were left on the hotplate to naturally cool down.

O_2-plasma treatment. After cooling down to room temperature, the NiO_x films were transferred to a plasma cleaning chamber (PE-50, Plasma Etch, Inc) and treated with O_2-plasma with different powers for 2 min. The O_2 flow rate was 10 sccm, and the chamber pressure was maintained at 300 Torr.

KCl passivation. KCl aqueous solutions were prepared at various concentrations from 5 to 20 mg/mL. The KCl solutions were filtered using a 0.45 μm PTFE filter, spin-coated onto the annealed NiO_x films at 3000 rpm for 30 s, and then dried on a hotplate at 150 °C for 5 min. After cooling down, the samples were transferred to the plasma machine and treated with O_2-plasma.

Device Fabrication

Perovskite solar cells (PSCs) were fabricated with the structure of ITO/NiO_x/ Perovskite/PCBM/BCP/Ag. The patterned ITO coated glass substrates were ultrasonically cleaned with deionized water, acetone, and isopropanol for 20 min in each solvent. NiO_x films were deposited on the cleaned ITO substrates, and different post-deposition treatments were performed. The samples were then transferred to a nitrogen-filled glovebox to prepare the perovskite layers. The $MA_{0.65}FA_{0.35}PbI_3$ perovskite precursor solution was prepared according to our previous report[2]. MAI (0.975 mmol), FAI (0.525 mmol), and PbI_2 (1.5 mmol) were dissolved in 1 mL mixed solvent of DMSO and DMF with a volume ratio of 1:9. Additional $Pb(SCN)_2$ with a molar ratio of 2.85% was added into the perovskite precursor solution. The precursor solution was stirred at 60 °C overnight and filtered using a 0.45 μm PTFE filter before use. Perovskite absorber layer was deposited by spin-coating 70 μL perovskite precursor at 500 rpm for 3s and 4000 rpm for 60 s. 750 μL of DE, as the anti-solvent agent, was dripped on the spinning substrate at the 5 s of the second step. The as-prepared perovskite films were annealed at 60 °C for 2 min and 100 °C for 7 min. After the samples cooling to room temperature, a 20 mg/ml PCBM in chlorobenzene solution was spin-coated at 2000 rpm for 30 s. An ultra-thin layer of BCP was prepared by spin-coating a BCP solution (0.5 mg/ml in anhydrous ethanol) at 4000 rpm for 30 s. Both layers were each annealed at 90 °C for 10 min. Finally, an 80 nm thick silver contact was evaporated at 3×10^{-7} torr to complete the fabrication process. The active area of devices is 0.12 cm^2 as defined by the overlapped region between the back electrode and the pre-patterned ITO.

Characterization

Transmittance spectra of NiO_x films were measured using an ultraviolet–visible (UV–vis) spectrophotometer (Lambda 1050, PerkinElmer) in a wavelength range of 300~900 nm. The reflection (R) spectra was obtained use the same machine with an integrating sphere, and the optical absorption of the films was calculated by A=100-(T+R) method. Film thickness was obtained by analyzing spectroscopic ellipsometry data collected using single rotating compensator multichannel ellipsometers (Model M2000FI and IR-VASE, J. A. Woollam Co., Inc.). X-ray photoelectron spectroscopy (XPS) and ultraviolet photoelectron spectroscopy (UPS) were performed using an XPS/UPS system (ESCLAB 250Xi, Thermo Scientific). The composition and binding state of NiO_x were determined by XPS using a monochromatic Al K_α radiation as the excitation source with a pass energy at 150 eV and a channel width of 500 meV. All the spectra were fitted with chemically reasonable and previously assigned components, and maintained consistent FWHM (full width at half maximum) values for each individual peak meanwhile. UPS was carried out using He I_α radiation from a discharge lamp operated at 90 W, a pass energy of 10 eV, and a channel width of 25 meV. The work function (WF) can be calculated by the equation of $E_F = 21.22 - E_B$, where the E_F is the Fermi level and the E_B is the cutoff in high binding energy range. The film morphology, surface element analysis and the device cross-sectional structure were observed using a Hitachi S-4800 high-resolution field emission scanning electron microscope (FE-SEM) equipped with energy-dispersive X-ray spectroscopy (EDS) system. The crystal structure of the NiO_x films and the perovskite deposited on NiO_x were examined by Grazing incidence X-ray diffractometer (GIXRD) and XRD respectively by Ultima III

(Rigaku Corp.) with Cu K_α radiation under operating conditions of 40 kV and 44 mA. Atomic force microscopy (AFM) images were acquired on a Veeco Nanoscope IIIA instrument operated in the tapping mode. The work function (contact potential difference) was conducted on a Kelvin probe system (KP020, KP Technology) in air. The steady-state photoluminescence (PL) and time-resolved photoluminescence (TRPL) was obtained with Delta Flex fluorescence spectrum spectroscopy (HORIBA) with an excitation laser wavelength of 481 nm. The current density-voltage (*J-V*) properties were characterized using a Keithley 2400 source meter under standard AM 1.5G illumination using a solar simulator (PV Measurements Inc.) equipped with a 450 W Xenon lamp (Newport Corp.) with an output intensity of 100 mW cm^{-2} calibrated with a reference Si cell at the measurement location. External quantum efficiency (EQE) measurement were performed on a spectral response system (model IVQE8-C QE system, PV Measurements Inc.) using 100 Hz chopped monochromatic light ranging from 300 to 850 nm under near-dark test conditions. The film (lateral) resistivity (ρ) was calculated from the linear sweep voltammetry curves measured under dark condition via the equation of $\rho=Rwt/L$, where R is the film resistance, w is the electrode width (4 mm), t is the film thickness (25 nm), and L is the channel length (2 mm). The carrier density was obtained by a Hall measurement system (Model 7707A, Lake Shore) in a van der Pauw geometry, the film thickness is 100 nm. The trap-filled limit voltages (V_{TFL}) of perovskite deposited on different NiO_x were obtained from the dark current-voltage (*I-V*) analysis. The device structure used there is ITO/NiO_x/perovskite/spiro-OMeTAD/Au. The curves usually consist three distinguishable segments: the linear ohmic region at low bias voltage, the trap filling transition (TFT) at the intermediate range where the current injection presents a marked increase, and then the space charge limited current (SCLC) regime[3, 4]. The kink point between the first two regions is defined as the trap-filling limit voltage (V_{TFL}), and the trap density (N_d) in device therefore could be calculated though the equation of $V_{TFL} = eN_dL^2/2\varepsilon\varepsilon_0$, where e presents the elementary charge of the electron, ε stands for the relative dielectric constant of perovskite (equal to 28.8 according to the references[5]), ε_0 is the vacuum permittivity and L is the thickness of our perovskite films (650 nm estimated from the cross-section SEM image). All the characterizations were measured in the ambient at room temperature.

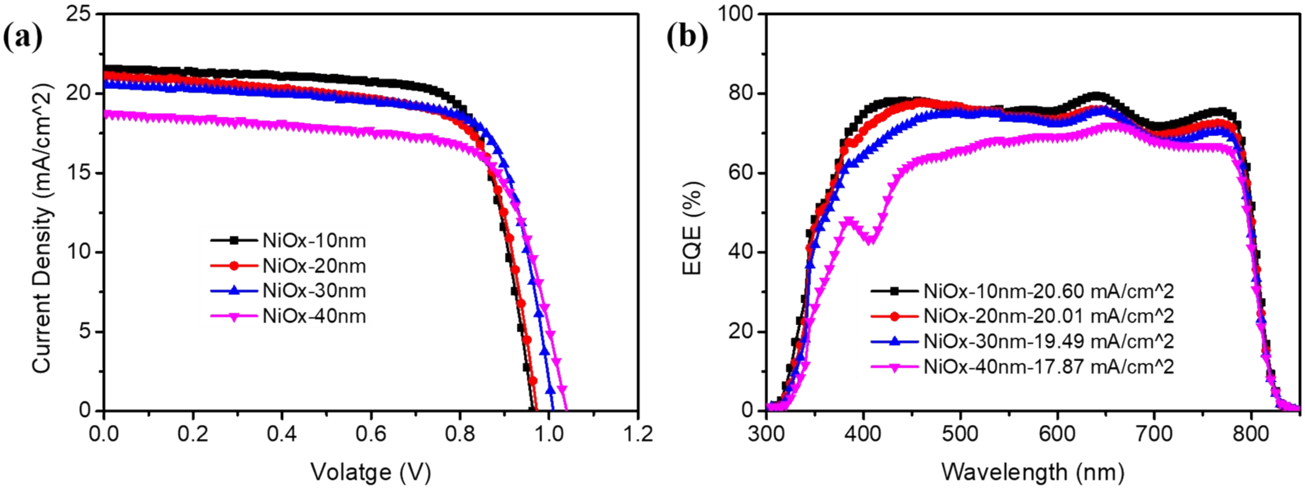

Figure S1. a) *J-V* curves and b) EQE spectra of the perovskite solar cells with different NiO_x layer thicknesses. *J-V* scans were recorded under the reversed voltage scan. The relevant paraments are summarized in Table S2.

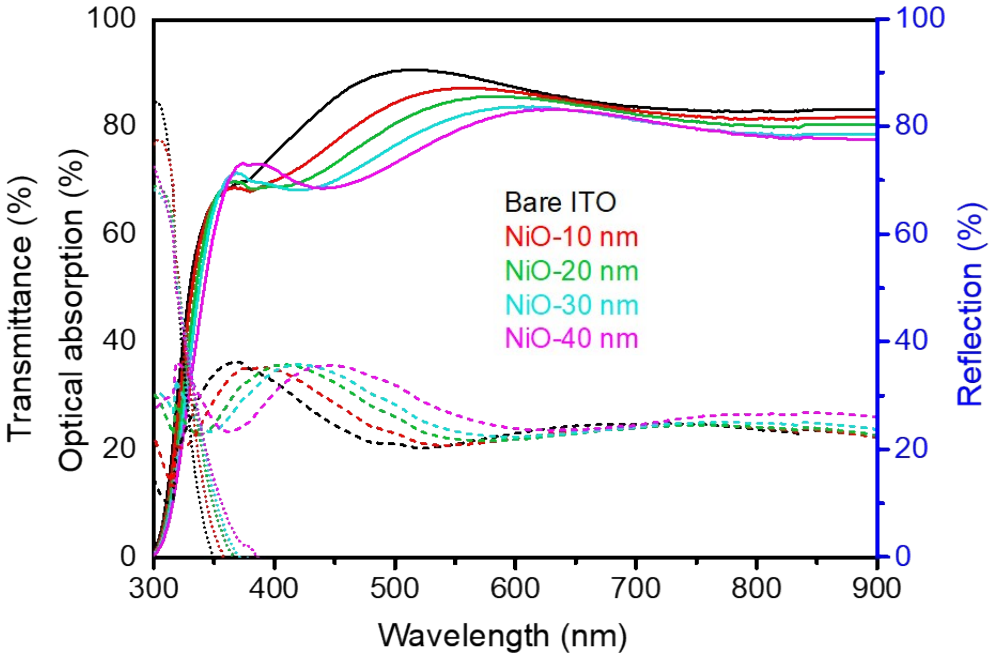

Figure S2. Transmittance (T), optical absorption (A), and reflection (R) spectra of the NiO_x films with different thicknesses.

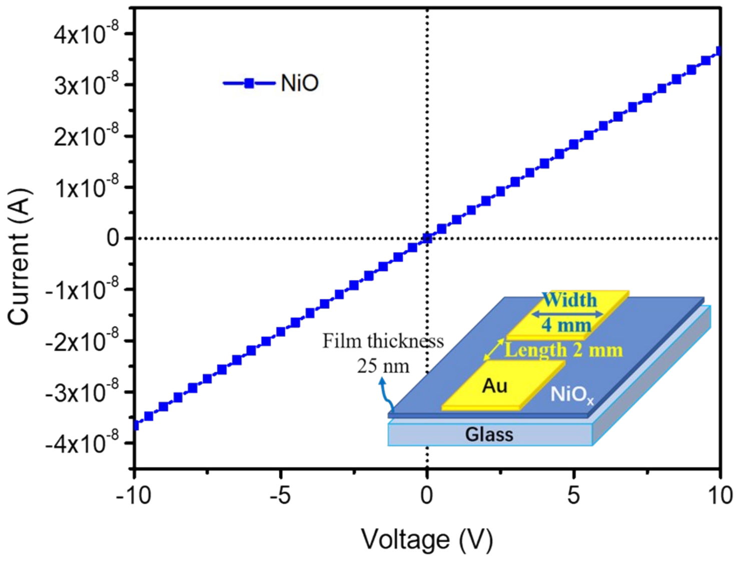

Figure S3. Linear sweep voltammetry (LSV) curve of the NiO$_x$ film. The device structure used for the test is given in the inset.

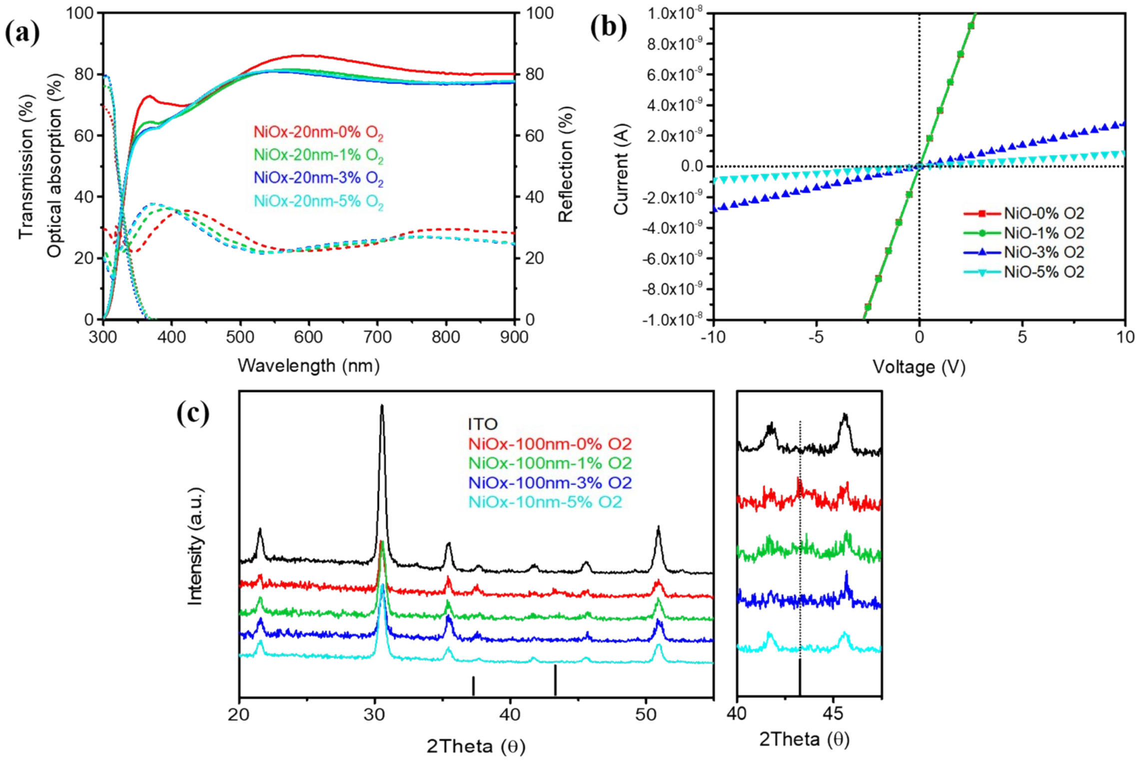

Figure S4. (a) Transmission, absorption and reflection spectra, (b) Linear sweep voltammetry curves, (c) GIXRD patterns of the NiO$_x$ film sputtered under different oxygen partial pressure.

To introduce extra oxygen into the NiO$_x$ film to promote the formation of V_{Ni}'', we first consider the possibility of improving the electrical properties of NiO_x film by applying an oxygen-rich sputtering atmosphere. However, this approach seems created an opposite effect in our case. **Figure S4** shows that the obtained film transmittance decreased obviously even within a 1% oxygen partial pressure environment. Further increase in the oxygen partial pressure no longer affected the transmittance but decreased the film resistivity significantly. Besides, the oxygen-rich environment also reduced the crystallinity of sputtered NiO_x film. These results reveal that the oxygen-rich sputtering atmosphere cannot promote the formation of V_{Ni}'' thus cannot improve the electrical properties of the NiO_x film.

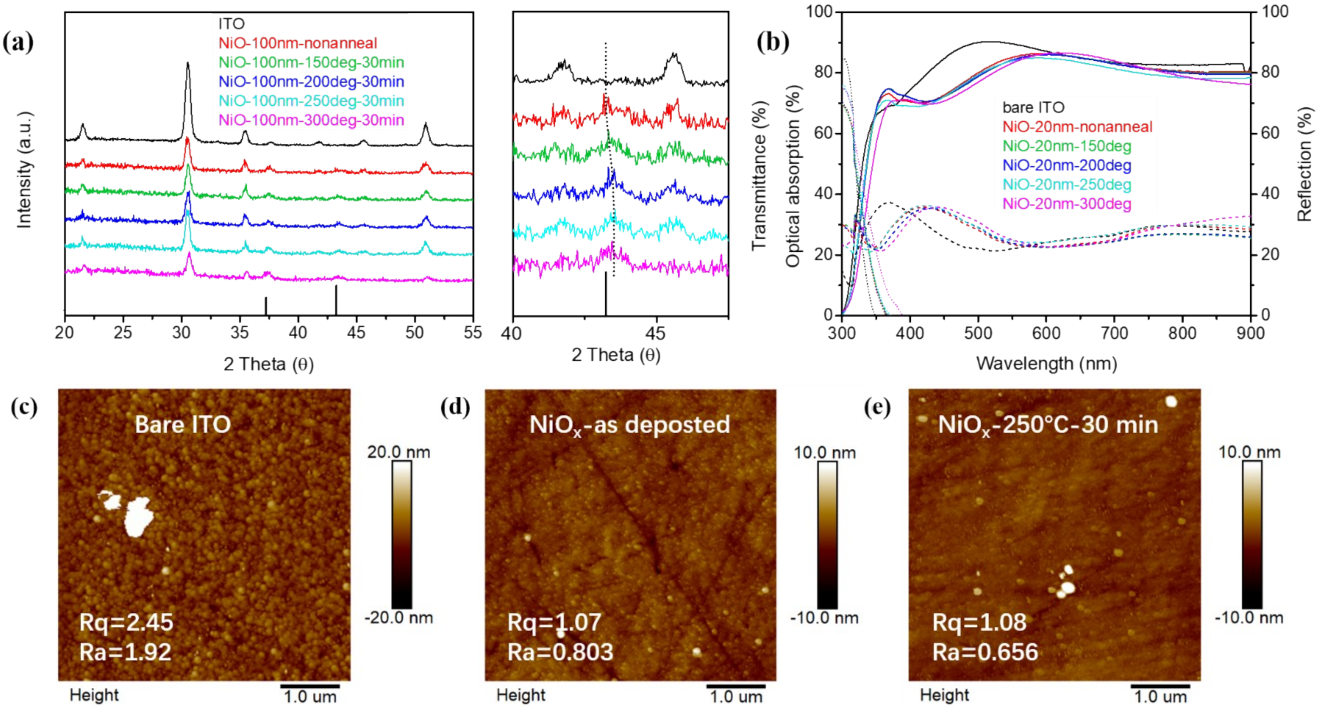

Figure S5. a) GIXRD patterns, b) Transmittance, optical absorption, and reflection spectra of the NiO_x films annealed at different temperatures. AFM topographic images of c) bare ITO, d) as-deposited NiO_x film, and e) NiO_x films after 250 °C annealing.

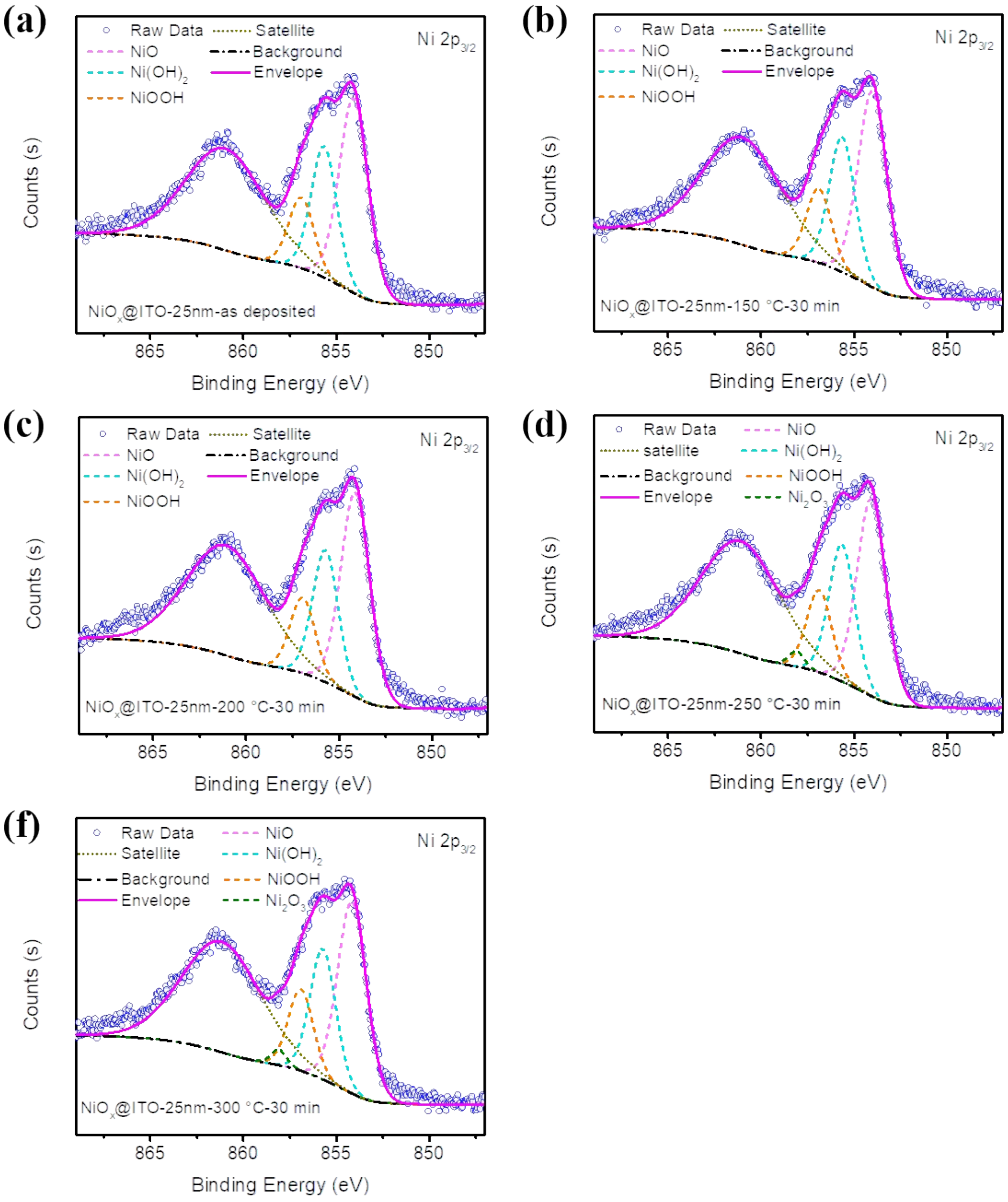

Figure S6. XPS spectra of Ni $2p_{3/2}$ state for NiO_x films annealed at different temperatures.

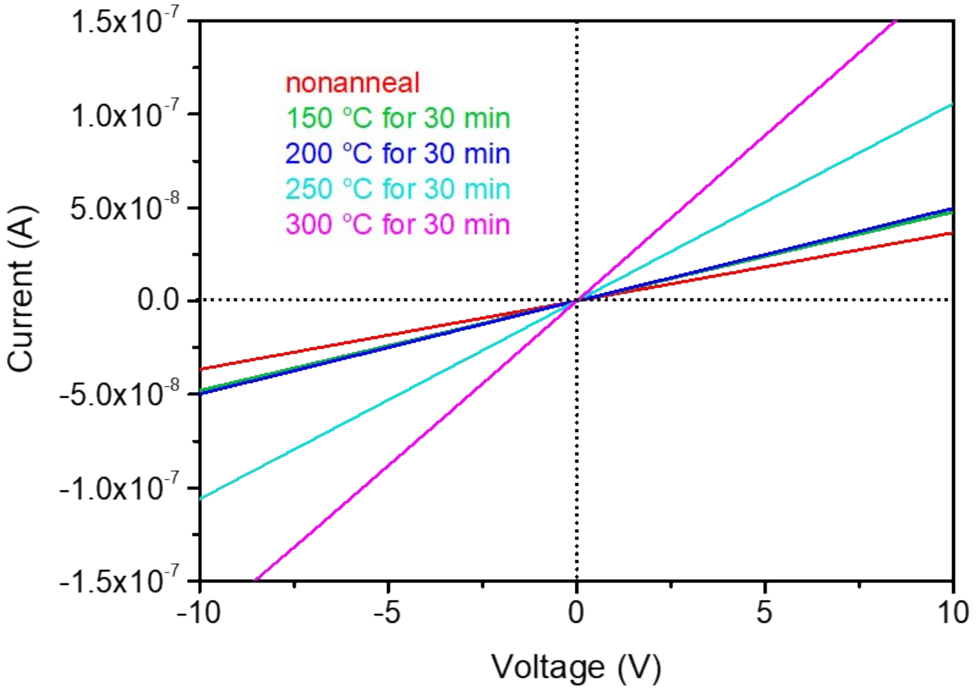

Figure S7. Linear sweep voltammetry curves of the NiO_x films annealed at different temperatures.

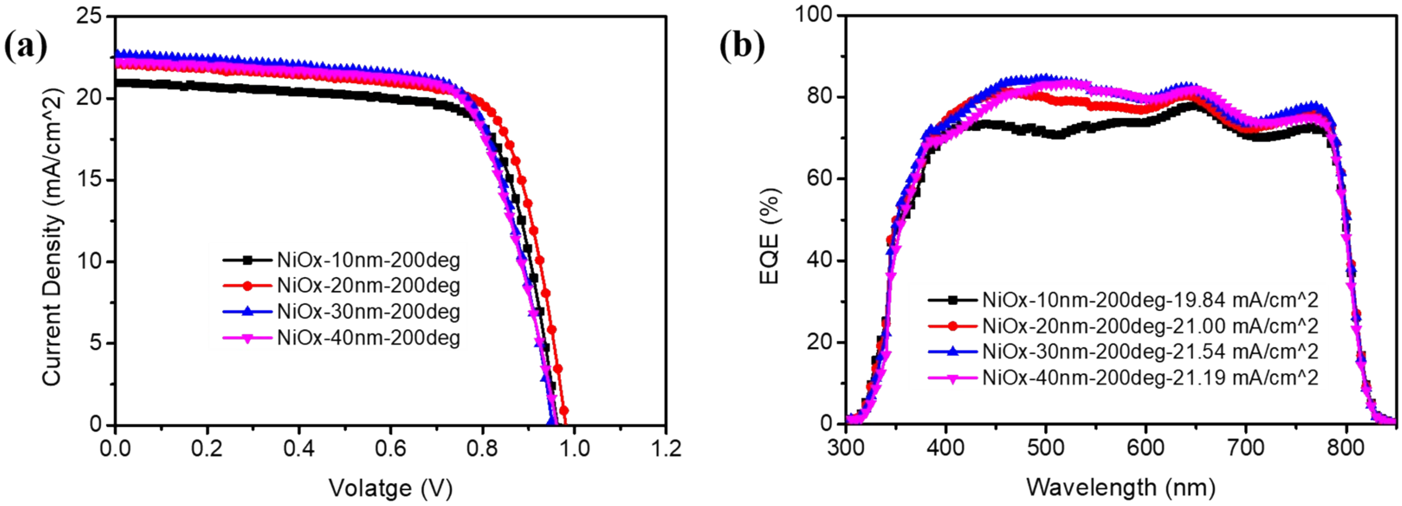

Figure S8. a) *J-V* curves under the reverse scans and b) EQE spectra of the perovskite solar cells with different NiO_x layer thicknesses. The NiO_x films were annealed at 200 °C for 30 min. The relevant paraments are summarized in Table S4.

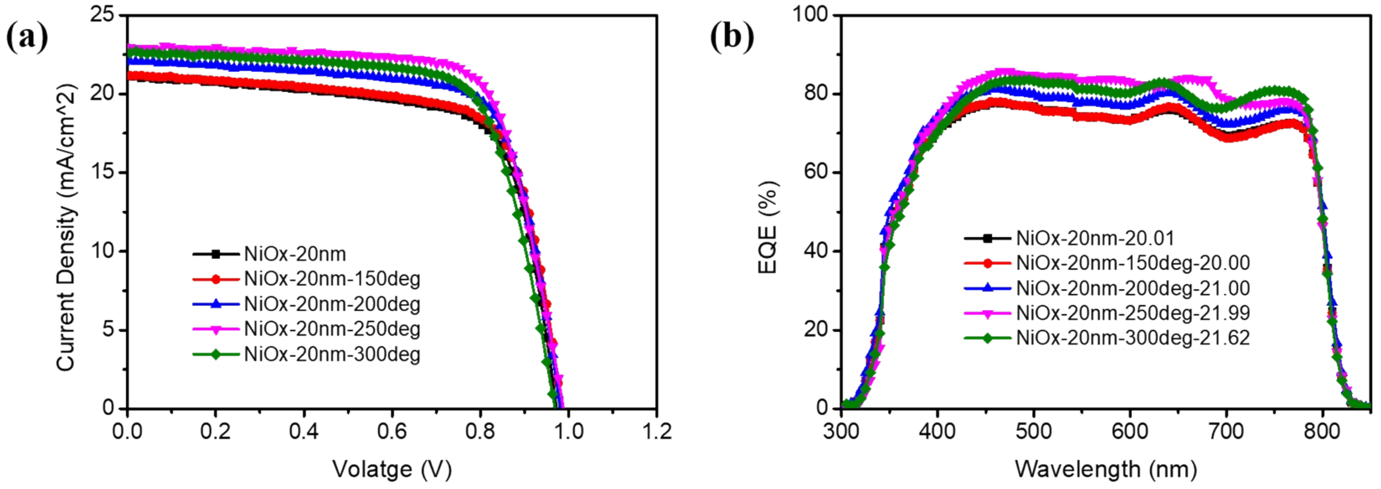

Figure S9. a) *J-V* curves under the reverse scans and b) EQE spectra of the perovskite solar cells with 20 nm NiO_x films annealed at different temperatures. The relevant paraments are summarized in Table S5.

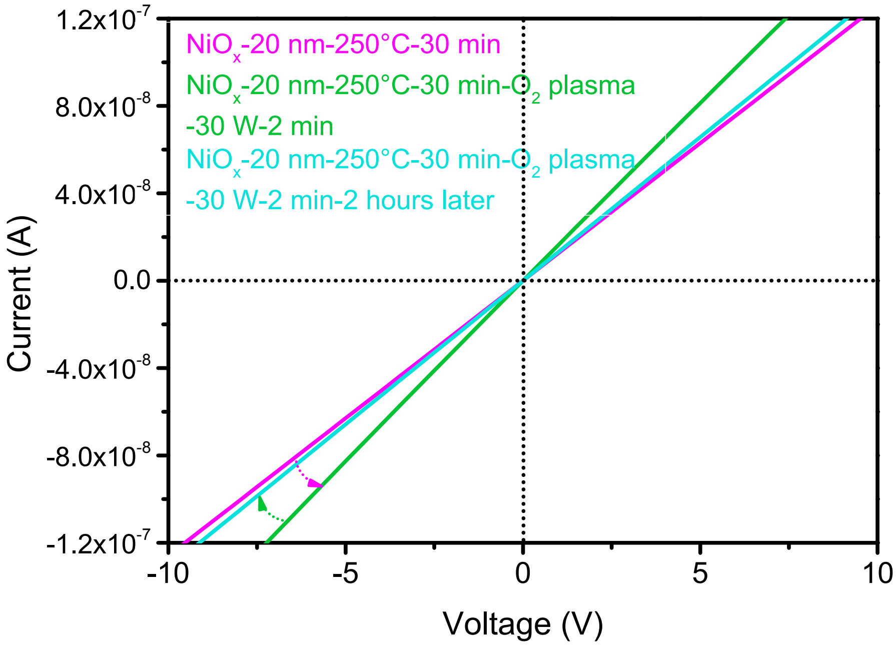

Figure S10. Transience of O_2-plasma treatment reflected in the fast recover of film resistance measured by the LSV measurements.

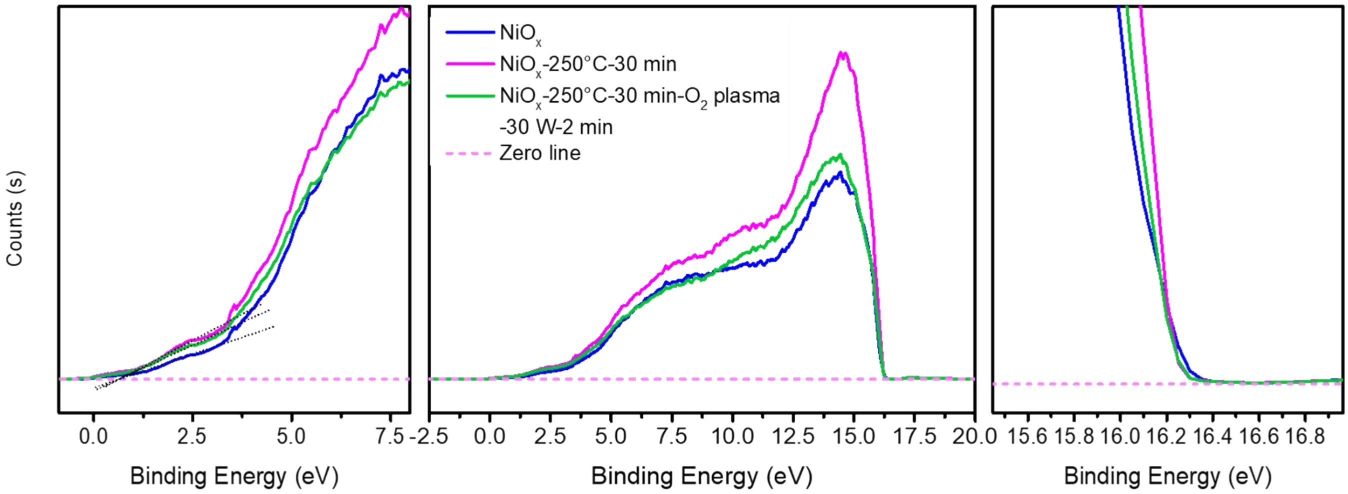

Figure S11. UPS spectra of the as-deposited, annealed, and annealed plus O_2-plasma treated NiO_x films. The magnified images of the low (left panel) and high (right panel) binding energy onsets are also shown.

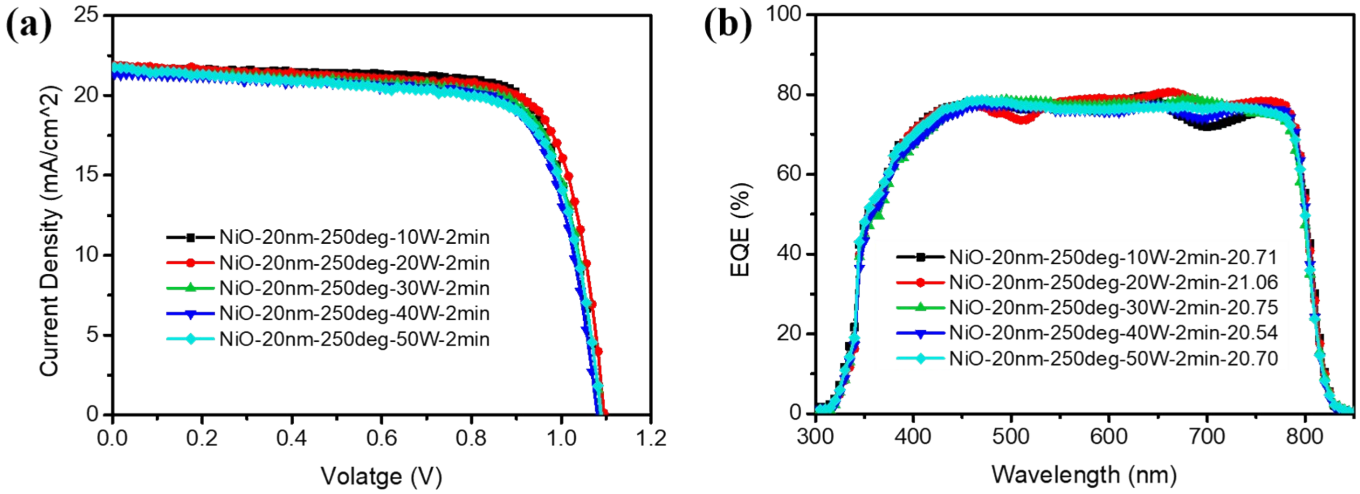

Figure S12. a) *J*-*V* curves under reverse scans and b) EQE spectra of the perovskite solar cells with annealed NiO_x films treated with O_2-plasma at different powers. The relevant paraments are summarized in Table S6.

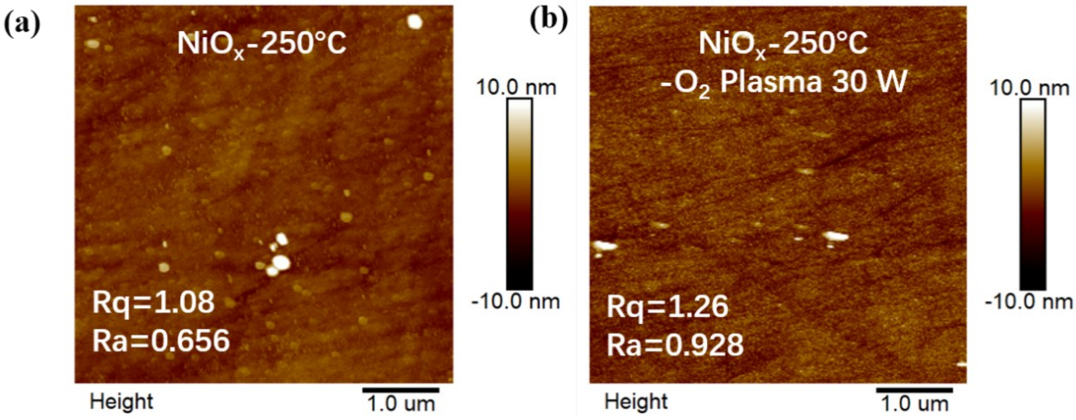

Figure S13. AFM topographic images of the annealed NiOx film surfaces a) without and d) with the O_2-plasma treatment.

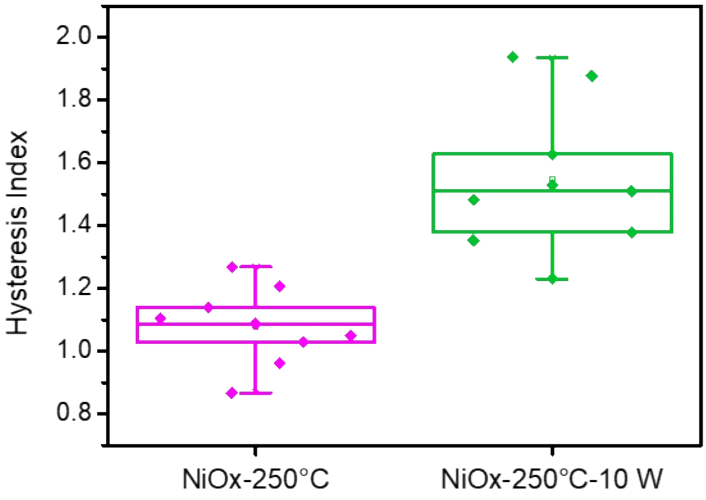

Figure S14. Hysteresis index statistic of the PSCs based on the annealed NiO_x HTLs with and without the O_2-plasma treatment. The hysteresis index was calculated by the equation of Hysteresis index = $PCE_{\text{Reverse scan}} - PCE_{\text{Forward scan}}$.

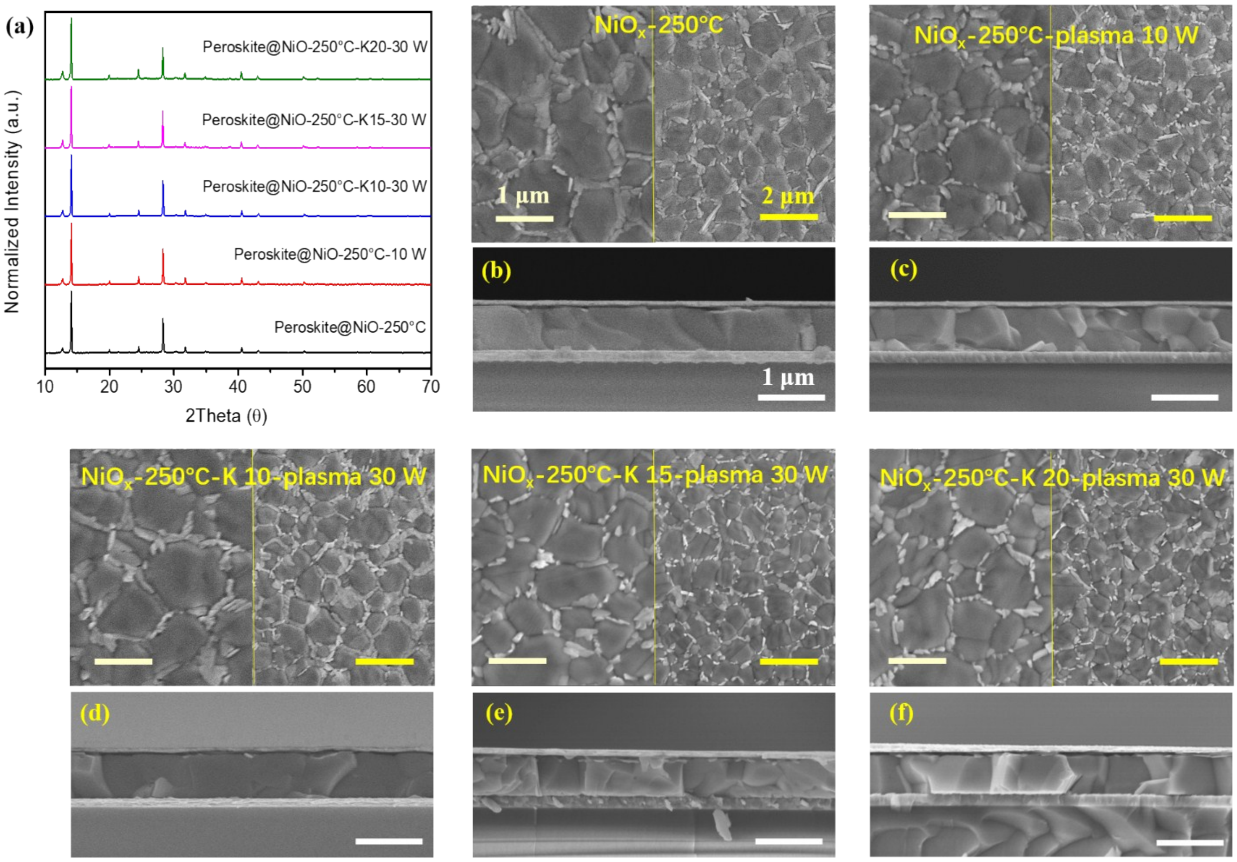

Figure S15. XRD patterns and SEM images (up: top-view; down: cross-sectional) of the perovskite films deposited on various NiO$_x$ films. The XRD patterns were normalized based on the relatively constant of (100) lattice plane of the perovskite. The bright particles that aggregated at the grain boundaries are considered to be PbI$_2$ crystals, which can be verified by the XRD pattens and is consistent with the literature[2, 6]. These excess PbI$_2$ are reported could passivate the defect and exhibit beneficial effects on cell performance.

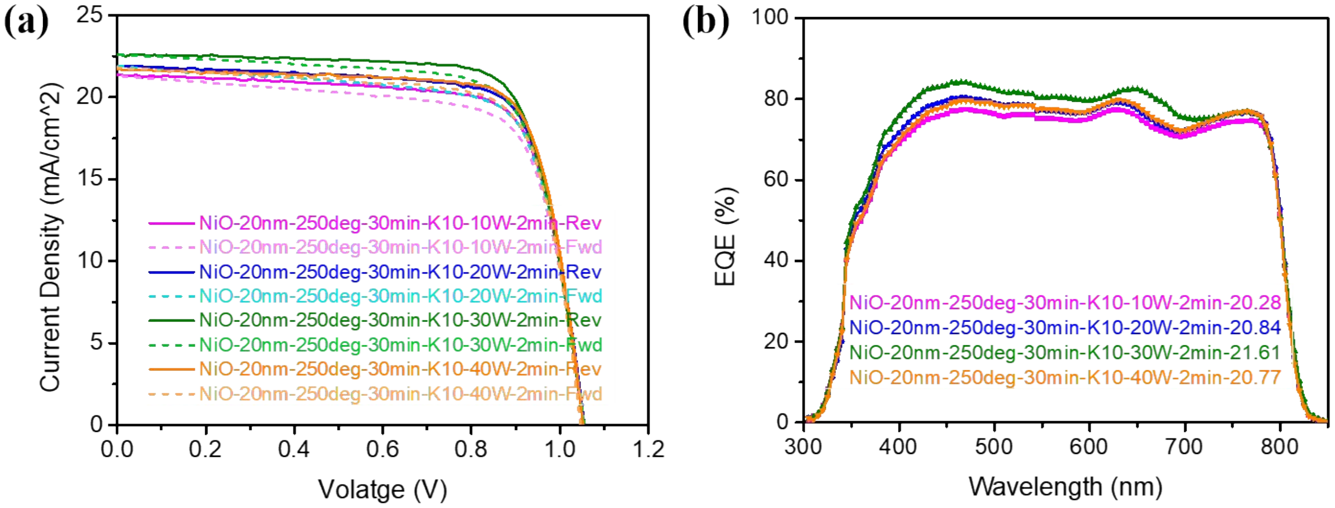

Figure S16. a) *J*-*V* curves and b) EQE spectra of the perovskite solar cells with the annealed NiO_x films treated with 10 mg/ml KCl and different plasma powers. The relevant paraments are summarized in Table S7.

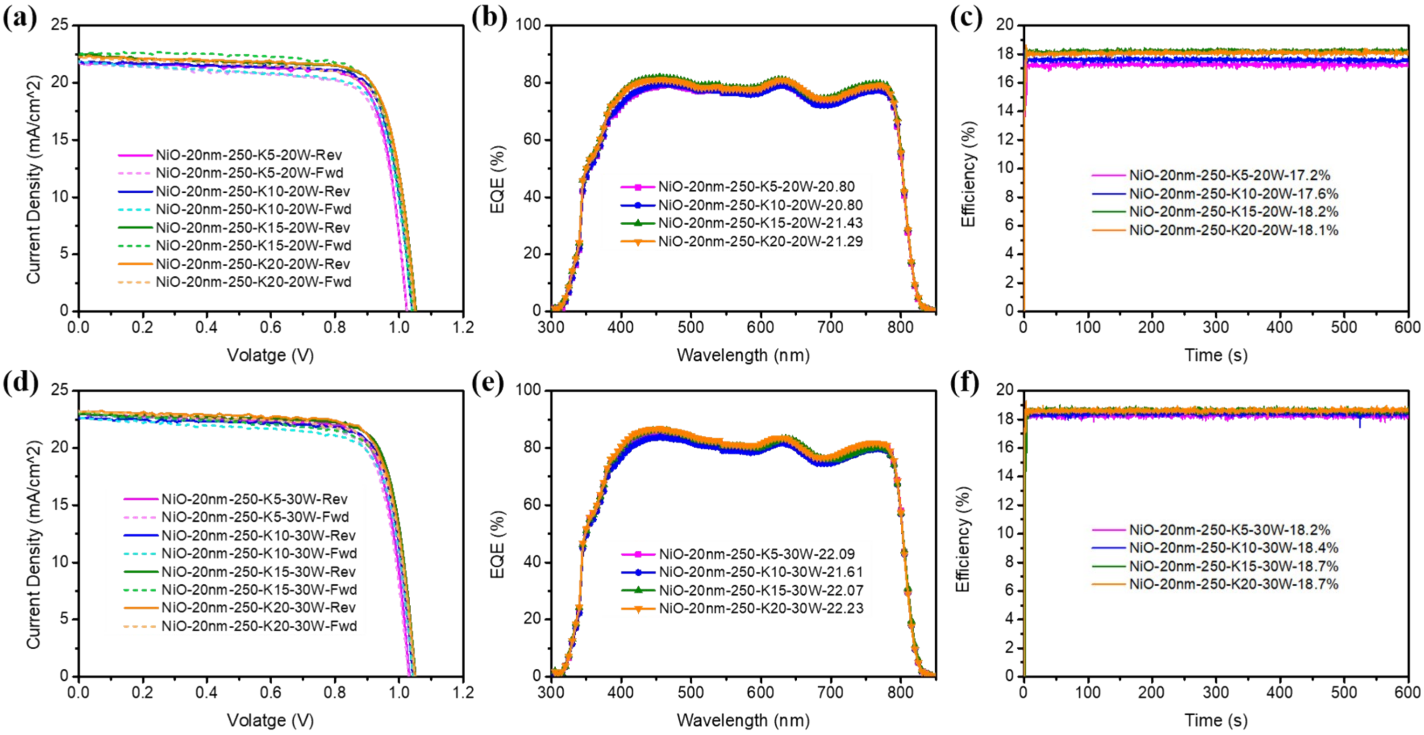

Figure S17. a), d) *J*-*V* curves, b), e) EQE spectra, and c), f) steady-state efficiencies of the perovskite solar cells with annealed NiO_x films treated with different KCl concentrations and plasma powers. The relevant paraments are summarized in Table S8.

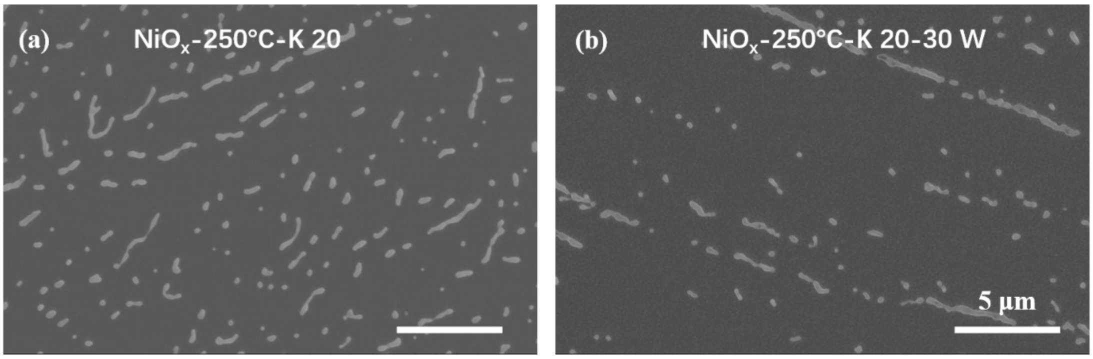

Figure S18. SEM images of the annealed and KCl (20 mg/ml) covered NiO$_x$ films with and without the O_2-plasma treatment.

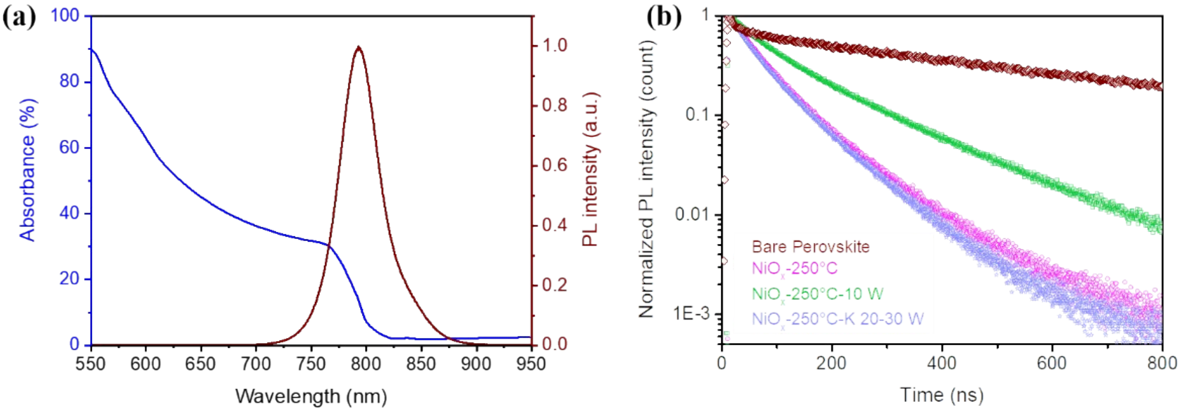

Figure S19. (a) Steady-state PL spectrum and absorbance of a bare perovskite film, (b) TRPL spectra of perovskite layers deposited on glass and three different NiO$_x$ films.

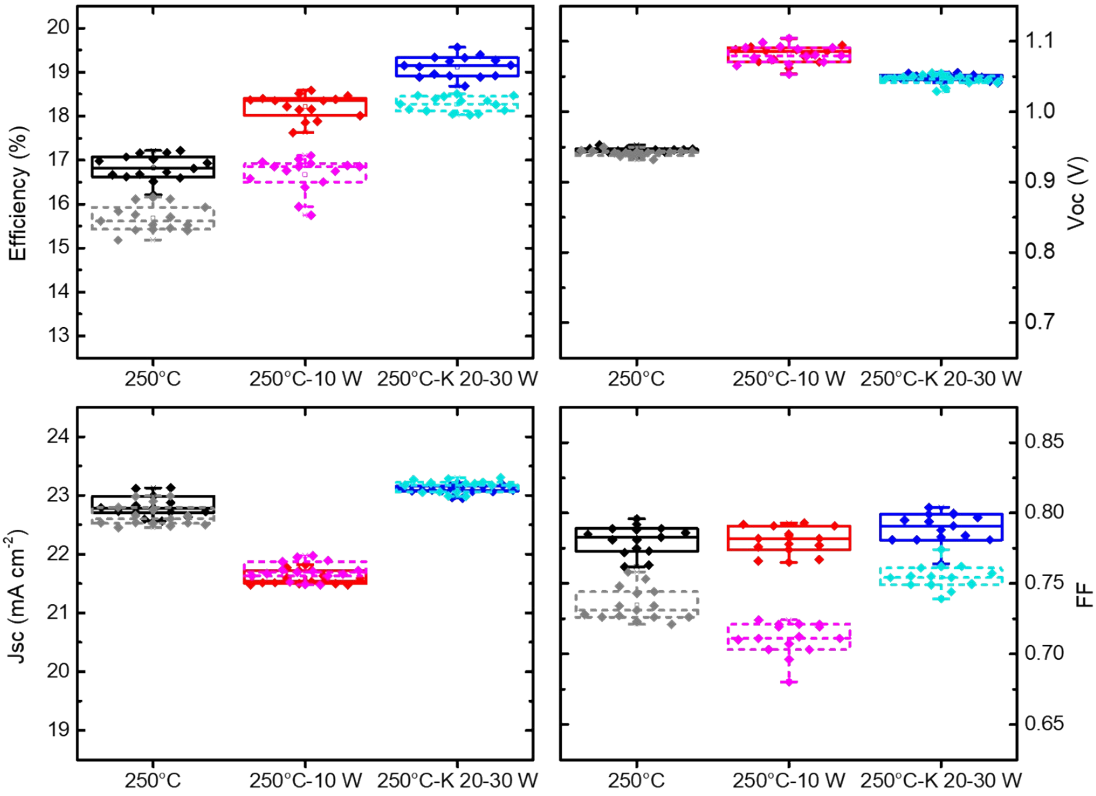

Figure S20. Statistical distribution of main photovoltaic parameters of the PSCs based on NiO_x-250 °C, NiO_x-250 °C-10 W, and NiO_x-250 °C-K 20-30 W HTLs.

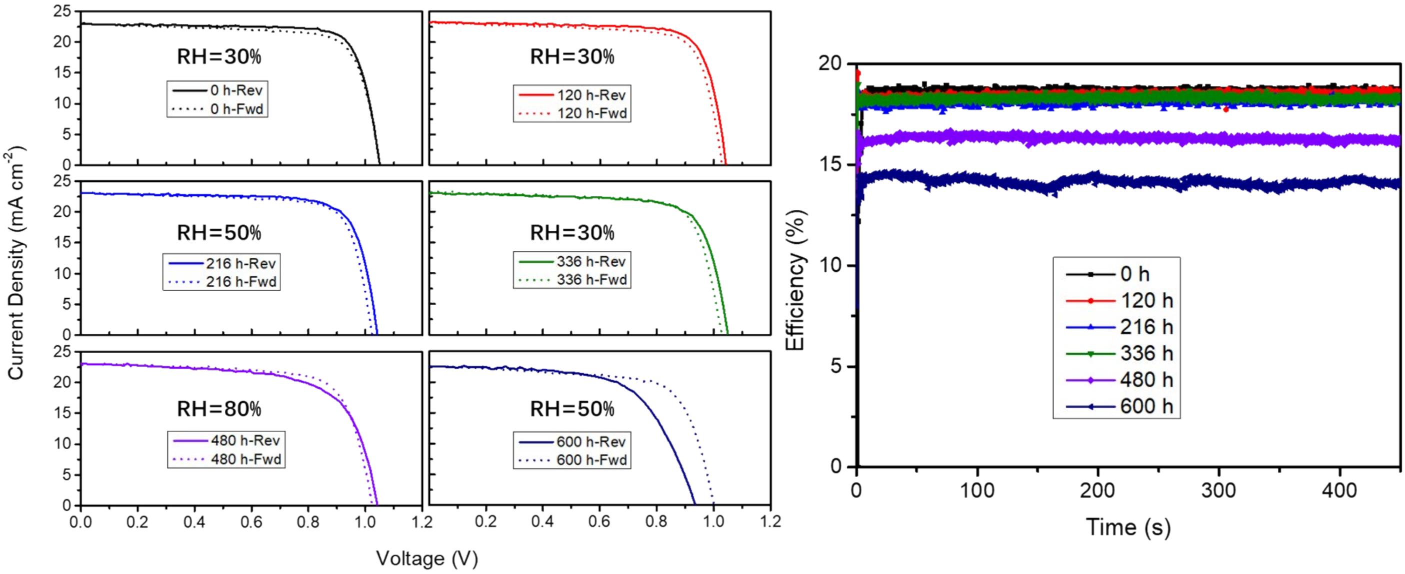

Figure S21. *J-V* curves and steady-state e□ciencies of a PSC based on the optimized HTL (NiO_x-250 °C-K 20-30 W) stored in dark and ambient air and tested periodically. The relevant paraments are summarized in Table S10.

Table S1. Summary of the optical parameters of sputtered NiO_x film.

	Film thickness [nm]	E_g [a] [eV]	WF [b] [eV]	E_F-E_V [b] [eV]	E_V [eV]	E_c [c] [eV]
NiO_x	20	3.63	4.85	0.5	-5.35	-1.72

[a] The band gap (E_g) value was extracted from the film's UV-Vis spectrum;

[b] The work function (WF) was calculated via the equation: $E_F = 21.22 - E_B$, where E_F is the Fermi level and E_B is the cutoff of UPS spectrum in high binding energy range; and the difference between the valence band maximum (E_V) and E_F were extracted from the cutoff of UPS spectrum in low binding energy range;

[c] The conduction band minimum (E_c) was calculated via the equation of $E_c = E_V + E_g$.

Table S2. *J-V* parameters of PSCs with different NiO_x thicknesses.

NiO_x thickness	V_{oc} [V]	J_{sc} [mA cm^{-2}]	FF	PCE [%]	$J_{integral}$ [a] [mA cm^{-2}]
10 nm	0.964	21.52	0.739	15.33	20.60
20 nm	0.972	21.14	0.707	14.53	20.01
30 nm	1.009	20.55	0.728	15.10	19.49
40 nm	1.040	18.75	0.699	13.63	17.87

[a] The integrated photocurrent density ($J_{integral}$) was calculated from the corresponding EQE spectrum;

[b] The active area of these devices are 0.12 cm^2;

[c] The data were extracted from the *J-V* curves under reverse scan direction.

Table S3. Binding energies and component ratios in the NiO_x films with different post treatments.

Ni $2p_{3/2}$		NiO	$Ni(OH)_2$	NiOOH	Ni_2O_3	satellite
FWHM (eV) [a]		1.84	1.63	1.58	0.96	5
w/o	Peak position (eV)	854.06	855.66	856.87		860.96
	Component ratio (%)	52.24	31.40	**16.37** [c]		
150 °C [b]	Peak position (eV)	854	855.64	856.89		861
	Component ratio (%)	51.61	31.64	**16.75**		
200 °C	Peak position (eV)	854.12	855.73	856.95		861.08
	Component ratio (%)	52.82	30.36	**16.82**		
250 °C	Peak position (eV)	854.06	855.65	856.87	858.1	861.09
	Component ratio (%)	49.59	30.65	**17.74**	**2.02**	
300 °C	Peak position (eV)	854.15	855.72	856.9	858.1	861.17
	Component ratio (%)	49.66	30.1	**18.1**	**2.14**	
250 °C-O_2 plasma-30 W	Peak position (eV)	854.12	855.66	856.85	858	861.15
	Component ratio (%)	48.89	29.8	**19.26**	**2.04**	

[a] All these spectra were fitted with chemically reasonable components and maintained consistent FWHM values for each individual peak meanwhile;

[b] The annealing time was fixed at 30 min;

[c] The bold numbers show the ratio of dipolar NiOOH component increased as the annealing temperature increase, and when the temperature up to 250 °C, the Ni_2O_3 specie present;

[b] All tested films were deposited on clean ITO substrate with a thickness of 25 nm.

Table S4. *J-V* parameters of PSCs with different NiO_x thicknesses. NiO_x films were annealed at 200 °C for 30 min.

NiO_x thickness	V_{oc} [V]	J_{sc} [mA cm^{-2}]	FF	PCE [%]	$J_{integral}$ [a] [mA cm^{-2}]
10 nm	0.963	20.9521	0.721	14.723	19.84
20 nm	0.981	22.07117	0.726	15.712	21.00
30 nm	0.952	22.64115	0.711	15.32516	21.54
40 nm	0.961	22.2277	0.706	15.094	21.19

[a] The $J_{integral}$ was calculated from the corresponding EQE spectrum;

[b] The active area of these devices are 0.12 cm^2;

[c] The data were extracted from the *J-V* curves under reverse scan direction.

Table S5. *J-V* parameters of PSCs based on 20 nm NiO_x films with different annealing temperatures.

Annealing temperature [a]	V_{oc} [V]	J_{sc} [mA cm^{-2}]	FF	PCE [%]	$J_{integral}$ [b] [mA cm^{-2}]
w/o	0.972	21.1354	0.707	14.526	20.01
150 °C	0.984	21.1949	0.712	14.85	20.00
200 °C	0.981	22.07117	0.726	15.712	21.00
250 °C	0.988	22.97058	0.73	16.5673	21.99
300 °C	0.969	22.62509	0.712	15.60968	21.62

[a] The annealing time was fixed at 30 min;

[b] The $J_{integral}$ was calculated from the corresponding EQE spectrum;

[c] The active area of these devices are 0.12 cm^2;

[d] The data were extracted from the *J-V* curves under reverse scan direction.

Table S6. *J-V* parameters of PSCs based on 20 nm NiO_x films with different O_2-plasma treatment powers.

Plasma power [a]	V_{oc} [V]	J_{sc} [mA cm^{-2}]	FF	PCE [%]	$J_{integral}$ [b] [mA cm^{-2}]
10 W	1.091	21.7253	0.766	18.149	20.71
20 W	1.095	21.8854	0.755	18.111	21.06
30 W	1.088	21.4875	0.75	17.541	20.75
40 W	1.080	21.3451	0.744	17.15	20.54
50 W	1.089	21.7846	0.723	17.157	20.70

[a] The NiO_x films were annealed at 250 °C for 30 min beforehand, and the plasma time was fixed at 2 min;

[b] The $J_{integral}$ was calculated from the corresponding EQE spectrum;

[c] The active area of these devices are 0.12 cm^2;

[d] The data were extracted from the *J-V* curves under reverse scan direction.

Table S7. *J-V* parameters of PSCs based on 20 nm NiO_x films with 10 mg/ml KCl solution [a] and different O_2-plasma treatment powers.

Plasma power [b]		V_{oc} [V]	J_{sc} [mA cm^{-2}]	FF	PCE [%]	$J_{integral}$ [c] [mA cm^{-2}]
10 W	Reverse	1.053	21.3769	0.751	16.901	20.28
	Forward	1.052	21.3385	0.722	16.202	
20 W	Reverse	1.055	21.9067	0.752	17.386	20.84
	Forward	1.055	21.8955	0.728	16.820	
30 W	Reverse	1.053	22.5848	0.764	18.163	21.61
	Forward	1.055	22.6143	0.732	17.469	
40 W	Reverse	1.053	21.7226	0.769	17.594	20.77
	Forward	1.047	21.8127	0.743	16.973	

[a] The NiO_x films were first annealed at 250 °C for 30 min, then spinning 10 mg/ml KCl solution on it (3000 rpm for 30 s) and drying at 150 °C for 5 min, finally treated with different O_2-plasma power;

[b] The plasma time was fixed at 2 min;

[c] The $J_{integral}$ was calculated from the corresponding EQE spectrum;

[d] The active area of these devices are 0.12 cm^2.

Table S8. *J-V* parameters of PSCs based on 20 nm NiO_x films with different KCl concentrations and O_2-plasma treatment powers [a].

KCl concentration [b]	Sweep	V_{oc} [V]	J_{sc} [mA cm^{-2}]	FF	PCE [%]	$J_{integral}$ [c] [mA cm^{-2}]
			20 W			
5 mg/ml	Reverse	1.024	21.7431	0.792	17.633	20.80
	Forward	1.024	21.7766	0.759	16.921	
10 mg/ml	Reverse	1.041	21.8257	0.792	17.988	20.80
	Forward	1.041	21.8702	0.755	17.178	
15 mg/ml	Reverse	1.052	22.4374	0.782	18.467	21.43
	Forward	1.044	22.5087	0.783	18.393	
20 mg/ml	Reverse	1.051	22.2906	0.787	18.437	21.29
	Forward	1.046	22.2186	0.767	17.834	
			30 W			
5 mg/ml	Reverse	1.032	22.9451	0.782	18.525	22.09
	Forward	1.029	22.9816	0.761	18.003	
10 mg/ml	Reverse	1.042	22.5953	0.792	18.659	21.61
	Forward	1.042	22.6575	0.755	17.832	
15 mg/ml	Reverse	1.051	22.9654	0.794	19.166	22.07
	Forward	1.050	23.0790	0.755	18.289	
20 mg/ml	Reverse	1.049	23.1704	0.788	19.158	22.23
	Forward	1.048	23.2141	0.761	18.510	

[a] The NiO_x films were first annealed at 250 °C for 30 min, then spinning KCl solution on it (3000 rpm for 30 s) and drying at 150 °C for 5 min, finally treated with O_2-plasma and the treated time was fixed at 2 min;

[b] The KCl concentration means the KCl concentration in solution;

[c] The $J_{integral}$ was calculated from the corresponding EQE spectrum;

[d] The active area of devices are 0.12 cm^2, and this batch devices were tested using a mask with 0.06 cm^2 area.

Table S9. Fitted carrier lifetimes and pre-factors [a] for perovskite deposited on different NiO_x substrates.

	PL peak (nm) [b]	b_1 [c]	τ_1 (ns) [d]	b_2	τ_2 (ns)	τ_{ave} (ns)
Bare perovskite	793	0	Null	1	635.00	635.00
NiO_x-250 °C	794	0.74	48.83	0.26	116.84	66.18
NiO_x-250 °C-10 W	793	0.56	66.82	0.44	188.59	120.31
NiO_x-250 °C-K 20-30 W	793	0.59	39.73	0.41	94.36	62.05

[a] The TRPL spectra were fitted by the biexponential function: $y=A+B_1*\exp(x/\tau_1)+B_2*(x/\tau_2)$, where A, B_1 and B_2 are the pre-factors;

[b] The peak position was extracted from the corresponding steady-state PL spectrum;

[c] The b_1 and b_2 are the normalized pre-exponential factors where $b_1=B_1/(B_1+B_2)$ and $b_2=B_2/(B_1+B_2)$, respectively;

[d] The τ_1 and τ_2 are the lifetimes of the fast and slow decay component, respectively, and $\tau_{ave}=b_1*\tau_1+b_2*\tau_2$.

Table S10. *J-V* parameters of PSCs based on the optimized HTL (NiO_x-250 °C-K 20-30 W) stored in dark and ambient air and tested periodically.

Aging time [h]	Relative humidity [%]	Sweep	V_{oc} [V]	J_{sc} [mA cm^{-2}]	FF	PCE [%]	MPP [%]
0	30	Reverse	1.051	22.9654	0.794	19.166	18.62
		Forward	1.051	23.1624	0.750	18.257	
120	30	Reverse	1.043	23.2128	0.781	18.918	18.53
		Forward	1.029	23.3029	0.757	18.156	
216	50	Reverse	1.043	23.0882	0.763	18.368	18.17
		Forward	1.024	23.0815	0.770	18.194	
336	30	Reverse	1.050	23.0033	0.752	18.142	18.32
		Forward	1.029	23.2205	0.752	17.973	
480	80	Reverse	1.042	23.0586	0.666	16.011	16.22
		Forward	1.024	22.9181	0.732	17.177	
600	50	Reverse	0.936	22.5111	0.631	13.385	14.02
		Forward	1.002	22.6522	0.702	15.943	

[a] The active area of the device are 0.12 cm^2, and it was tested using a mask with 0.06 cm^2 area.

References

1. E. Aydin, J. Troughton, M. De Bastiani, E. Ugur, M. Sajjad, A. Alzahrani, M. Neophytou, U. Schwingenschlögl, F. Laquai and D. Baran, *ACS Appl. Energy Mater.*, 2018, **1**, 6227-6233.
2. C. Wang, C. Xiao, Y. Yu, D. Zhao, R. A. Awni, C. R. Grice, K. Ghimire, I. Constantinou, W. Liao and A. J. Cimaroli, *Adv. Energy Mater.*, 2017, **7**, 1700414.
3. A. Carbone, C. Pennetta and L. Reggiani, *Appl. Phys. Lett.*, 2009, **95**, 233303.
4. X. Yin, J. Han, Y. Zhou, Y. Gu, M. Tai, H. Nan, Y. Zhou, J. Li and H. Lin, *J. Mater. Chem. A*, 2019, **7**, 5666-5676.
5. A. Poglitsch and D. Weber, *J. Chem. Phys.*, 1987, **87**, 6373-6378.
6. W. Ke, C. Xiao, C. Wang, B. Saparov, H.-S. Duan, D. Zhao, Z. Xiao, P. Schulz, S. P. Harvey, W. Liao, W. Meng, Y. Yu, A. J. Cimaroli, C.-S. Jiang, K. Zhu, M. Al-Jassim, G. Fang, D. B. Mitzi and Y. Yan, *Adv. Mater.*, 2016, **28**, 5214-5221.